



Gamma-Ray Spectrometry Analysis Methods for Radioisotope Dissolution and Mixing for Nuclear Forensics Applications

August 2022

Changing the World's Energy Future

Tommy V Holschuh, Mathew S Snow, Luis A Ocampo Giraldo, David L Chichester



DISCLAIMER

This information was prepared as an account of work sponsored by an agency of the U.S. Government. Neither the U.S. Government nor any agency thereof, nor any of their employees, makes any warranty, expressed or implied, or assumes any legal liability or responsibility for the accuracy, completeness, or usefulness, of any information, apparatus, product, or process disclosed, or represents that its use would not infringe privately owned rights. References herein to any specific commercial product, process, or service by trade name, trade mark, manufacturer, or otherwise, does not necessarily constitute or imply its endorsement, recommendation, or favoring by the U.S. Government or any agency thereof. The views and opinions of authors expressed herein do not necessarily state or reflect those of the U.S. Government or any agency thereof.

Gamma-Ray Spectrometry Analysis Methods for Radioisotope Dissolution and Mixing for Nuclear Forensics Applications

Tommy V Holschuh, Mathew S Snow, Luis A Ocampo Giraldo, David L Chichester

August 2022

**Idaho National Laboratory
Idaho Falls, Idaho 83415**

<http://www.inl.gov>

**Prepared for the
U.S. Department of Energy
Under DOE Idaho Operations Office
Contract DE-AC07-05ID14517**

1

Title page

2 Names of the authors: Tommy V. Holschuh, Luis A. Ocampo Giraldo, Mathew S. Snow,
3 David L. Chichester

4 Title: GAMMA-RAY SPECTROMETRY ANALYSIS METHODS FOR
5 RADIOISOTOPE DISSOLUTION AND MIXING FOR NUCLEAR FORENSICS
6 APPLICATIONS

7 Affiliation(s) and address(es) of the author(s): Idaho National Laboratory

8 1955 N. Fremont Avenue

9 PO Box 1625, MS2212

10 Idaho Falls, ID 83415

11 E-mail address of the corresponding author: Tommy.Holschuh@inl.gov

12

13 **NOTICE THIS IS A PART OF A SPECIAL ISSUE!!**

14 **SI: Methods and Applications of Radioanalytical Chemistry (MARC XII)**

15 **➔MARC XII Assigned Log Number: 505**

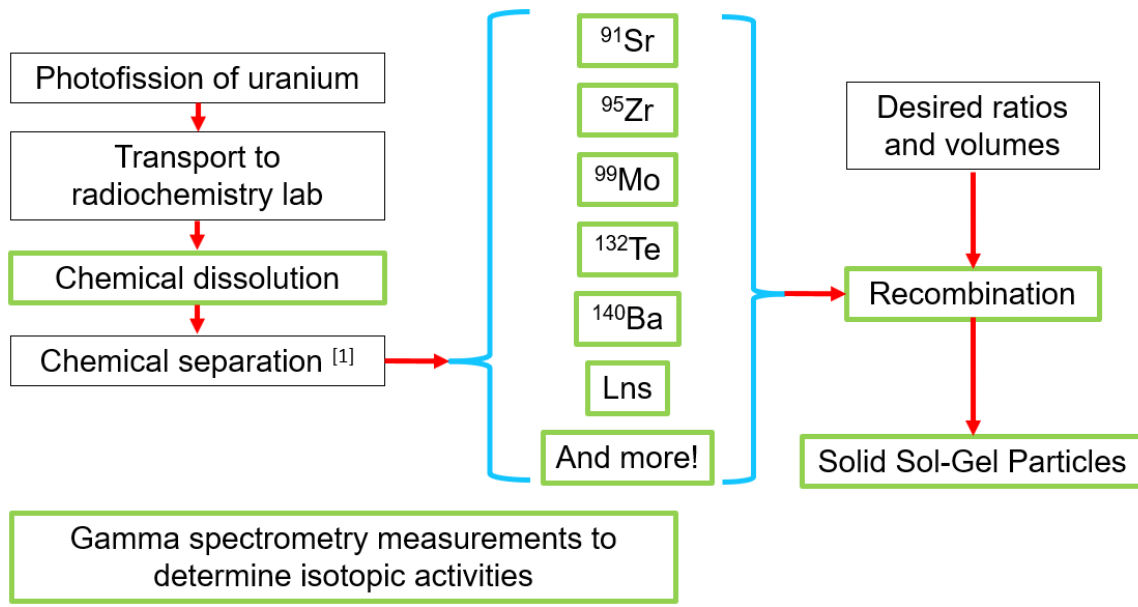
16

40 **Keywords**

41 Gamma-ray spectrometry, post-irradiation measurement, nuclear forensics, isotope
42 dissolution

43 **Introduction**

44 The nuclear forensics community requires training materials in lieu of realistic nuclear
45 explosive debris. Sol-gel glass provides numerous advantages as a surrogate debris, and
46 impregnation of radionuclides within the sol-gel allows customized design for particular
47 needs. Gamma spectrometry is used at several steps within the production process of sol-
48 gel to confirm radionuclide content and determine mixing volumes for future steps. For
49 gamma spectrometry to be correctly utilized, the detector efficiencies must be quantified
50 for varying geometries and stand-off distances that are based on a sample's activity.
51 Since radioactive laboratory standards cannot properly represent the radioactive sol-gel
52 samples, computational methods such as Monte Carlo N-Particle (MCNP) [1] are used to
53 compare simulated detector responses to laboratory calibration standards to provide
54 confidence in the ability for the detector model to represent measurements of radioactive
55 sol-gel particles in a vial. Then, the simulated detector efficiencies for sol-gel glass at
56 varying distances are used to calculate the measured activity and effective fissions (EF)
57 during each gamma-ray measurement along with nuclear data for half-life, photon yield
58 per disintegration, and fission yield for each isotope [2]. Figure 1 describes the process
59 flow for production of sol-gel glass particles. The boxes highlighted in green require
60 gamma spectrometry to be performed. The chemical separation into the various isotopes
61 (Lns = lanthanides) allows a variety of isotope ratios to be created during the liquid
62 recombination phase of the process for final creation of solid sol-gel particles.



63

64

Figure 1. Process for production of sol-gel glass particles

65

66 **Gamma-ray Spectrometry**

67 A high-purity germanium (HPGe) detector, the Oak Ridge Technical Enterprises
68 Corporation (ORTEC) Interchangeable Detector Module (IDM) shown in Figure 2, was
69 chosen for performing gamma spectrometry during the sol-gel process for several key
70 advantages. The planar, rather than co-axial, detector configuration increases the
71 resolution for photopeaks in the gamma-ray spectra. Additionally, the detector crystal
72 possesses a relatively high aspect ratio in terms of diameter to thickness, which decreases
73 its efficiency beyond approximately 1 MeV and prevents high energy photons from
74 increasing the Compton scattering within the crystal, benefiting the observations of
75 gamma-rays from desired fission products in the range of 200-800 keV.

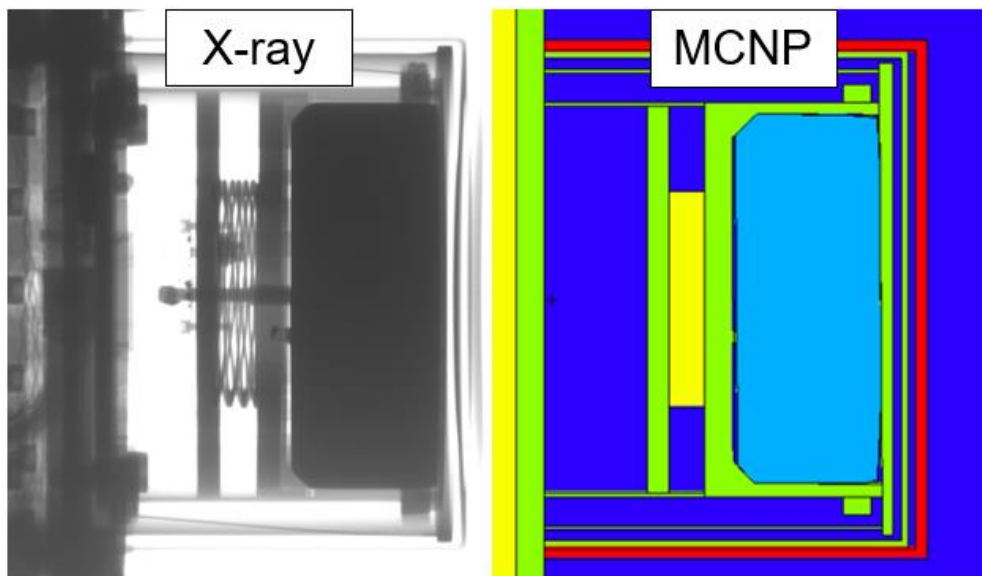
76 For accurate representation of the detector geometry in a computational model, x-rays are
77 taken upon receipt of the detector to identify dimensions and orientation of the crystal
78 and housing structures that affect the detector response. Figure 3 portrays two images of
79 the detector crystal with an x-ray image and an MCNP visual editor (VISED) rendering.
80 Note that the crystal is not cylindrical and contains chamfers on the rear and front of the

81 crystal. Additionally, the orientation of the crystal is perfectly aligned with the crystal
82 housing, and small screws are used to keep the crystal in place.



83

84 Figure 2. HPGe detector in measurement setup

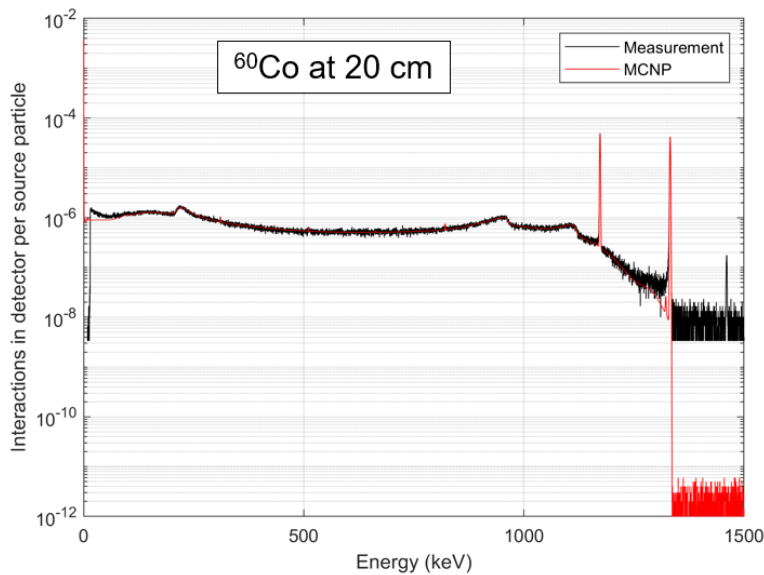


85

86 Figure 3. Comparison of detector geometry for ORTEC IDM detector

87 To provide confidence in an MCNP computational model of the detector's response,
88 radioactive laboratory standards are measured and simulated. In Figure 4, a comparison
89 of the measurement and MCNP simulation of ^{60}Co at a standoff distance of 20 cm is
90 shown. The peak agreement appears good, and most importantly, the Compton continua,
91 including single-escape peaks, are in good agreement. Small improvements can be made
92 in the overall agreement between the two spectra through incorporation of coincidence
93 summing effects for post-processing the MCNP simulation. The agreement in Figure 4

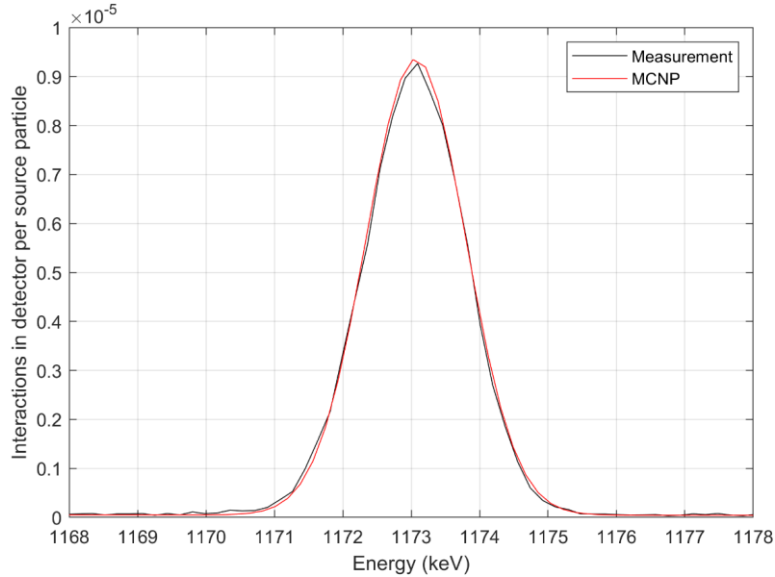
94 contains no “adjustments” or fudge factors to adjust the MCNP or detector gamma-ray
95 spectra, providing confidence for use of the detector simulations in scenarios with
96 radioactive samples with no viable laboratory standard. Figure 5 isolates the 1173 keV
97 photopeaks from Figure 4 on a linear, rather than logarithmic, to accentuate differences
98 between the two spectra. The agreement is very good in terms of photopeak height, full-
99 width half-maximum of the peak, and Table 1 presents numerical comparisons for the
100 photopeaks. The uncertainty on the laboratory standard is 1% with a coverage factor of 1
101 ($k = 1$, or 1σ), and the simulated response is within 2% of the laboratory standard. In
102 other words, the uncertainty in the difference between the two photopeak areas is larger
103 than the difference itself, which is the objective for performing detailed detector models.



104

105 Figure 4. Comparison of measurement and MCNP simulation results for ^{60}Co source

106



107

108 Figure 5. Peak comparison of measurement and simulation results for ⁶⁰Co source

109

110 Table 1. Comparison of measured and simulated detector responses

	Value	Uncertainty ($k = 2$)
Photopeak Counts (Measurement)	27699.6	336
Source Uncertainty	553.9	2% of Measured Photopeak Counts
Photopeak Counts (Simulation)	27302.8	334.8
Difference in Photopeak Counts	396.8	474.3

111 **Radioisotope Ratios**

112 From fission, a probabilistic distribution of fission products is created. The desired ratios
 113 of fission products for sol-gel are often different from natural distribution of fission.
 114 Additionally, different modes of fission (e.g., thermal reactor, fast fission) have different
 115 distributions of fission products. The creation of fission products for the sol-gel is
 116 performed with photon-induced fission induced by a linear accelerator, so the fission
 117 product yields are different than traditional thermal neutron-induced fission. The isotope
 118 ratios are defined in several different ways (Freiling R -value, little r -gamma, and R -
 119 gamma), shown in three equations in Figure 6 [3,4] with the variables shown in Table 2.
 120 When determining R -values during production of sol-gel values, the gamma-ray spectra

121 are used to calculate the number of atoms, N , or counts per minute, cpm , to be used in the
 122 isotope ratio. During preparation of the sol-gel glass, there is one additional factor that is
 123 necessary – total number of fission products in the sample. Since the method of fission
 124 used, photon-induced fission, is different than other types of fission, the fission product
 125 distributions are different. For normalization, ^{99}Mo is used as the standard when
 126 calculating (EF) and comparing the other isotopes.

$$FR_{ijk} = \frac{N_{jk}}{Y_{Ti}} \frac{N_{ji}}{Y_{Tk}} \quad r_{\gamma,ik} = \frac{(cpm/g)_i}{(cpm/g)_k} \quad R_{\gamma,ijk} = \frac{N_{ji}}{Y_{Ti}} \frac{N_{jk}}{Y_{Tk}}$$

127

128

Figure 6. Definition of various isotope ratios

129

130 Table 2. Variables used in Figure 6

Variable	Definition
j	Neutron spectrum (e.g., thermal, fast)
i	Volatile isotope of interest
k	Refractory isotope of interest
Y_T	Fission yield of isotope i from thermal fission of ^{235}U
N	Number of atoms projected to time in past or future
cpm	Counts per minute
g	Grams

131

132 **Matrix Inversion Mathematics**

133 The separation of fission products from the solution of all fission products is performed
 134 with a rapid radiochemical process [5]. Due to several factors, chemical separations are
 135 often imperfect, which introduces complexities during recombination of the separated

136 fission product solutions. If isotopes are completed separately, adding a vial of solution
 137 (e.g., molybdenum) only introduces molybdenum to the combined solution. However,
 138 with imperfect chemical separation, the addition of a molybdenum solution introduces
 139 molybdenum and several other isotopes, which impacts the isotope ratios in the final
 140 mixture. To address the imperfect chemistry, a matrix-based approach was found to
 141 quantify the isotopes of interest in each isotopic solution [6]. Figure 7 shows the matrix-
 142 based set up for the *R*-gamma calculations performed for a recombination mixture with
 143 the variables defined in Table 3. In the case of perfect chemical separations, the matrix in
 144 Figure 7 becomes a diagonal matrix. With the matrix-based approach, uncertainties in the
 145 gamma-ray spectra and nuclear data can be carried through to the final values of EF and
 146 *R*-gamma.

$$\begin{bmatrix} F_{Mo}^{Mo} & F_{Mo}^{Zr} & F_{Mo}^{Te} & F_{Mo}^{Ba} & F_{Mo}^{Nd} \\ D_{Zr}^{Mo} & D_{Zr}^{Zr} & D_{Zr}^{Te} & D_{Zr}^{Ba} & D_{Zr}^{Nd} \\ D_{Te}^{Mo} & D_{Te}^{Zr} & D_{Te}^{Te} & D_{Te}^{Ba} & D_{Te}^{Nd} \\ D_{Ba}^{Mo} & D_{Ba}^{Zr} & D_{Ba}^{Te} & D_{Ba}^{Ba} & D_{Ba}^{Nd} \\ D_{Nd}^{Mo} & D_{Nd}^{Zr} & D_{Nd}^{Te} & D_{Nd}^{Ba} & D_{Nd}^{Nd} \end{bmatrix} \begin{bmatrix} V_{Mo} \\ V_{Zr} \\ V_{Te} \\ V_{Ba} \\ V_{Nd} \end{bmatrix} = \begin{bmatrix} EF_{Mo} & R_{Zr/Mo} & R_{Te/Mo} & R_{Ba/Mo} & R_{Nd/Mo} \end{bmatrix}$$

147 Figure 7. Equation expressing the matrix form of solution with volumes and R-values
 148

149

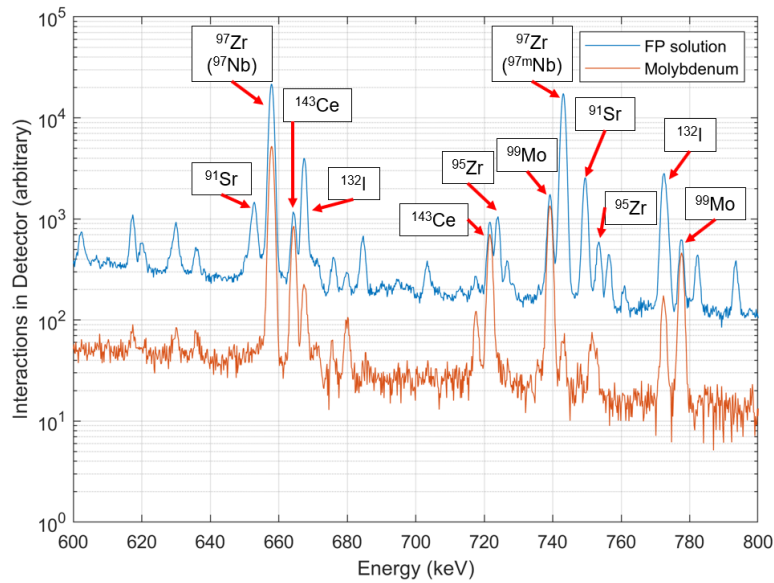
150 Table 3. Variables used in Figure 7

Variable	Definition
F_x^y	Fissions of isotope <i>x</i> in solution <i>y</i>
D_x^y	Atoms of isotope <i>x</i> in solution <i>y</i>
V_y	Volumes to be added from each solution <i>y</i>

151 Results

152 For the isotope ratios of interest for sol-gel production, the measurements of several
 153 gamma-ray spectra are shown in Figure 8, Figure 9, and Figure 10. The isotopic
 154 differences are illustrated in each figure. In Figure 8, the molybdenum solution (orange)
 155 is compared to the total fission product solution. The molybdenum solution contains Nb,
 156 Ce, Mo, and some iodine. The total solution contains all the molybdenum constituents in

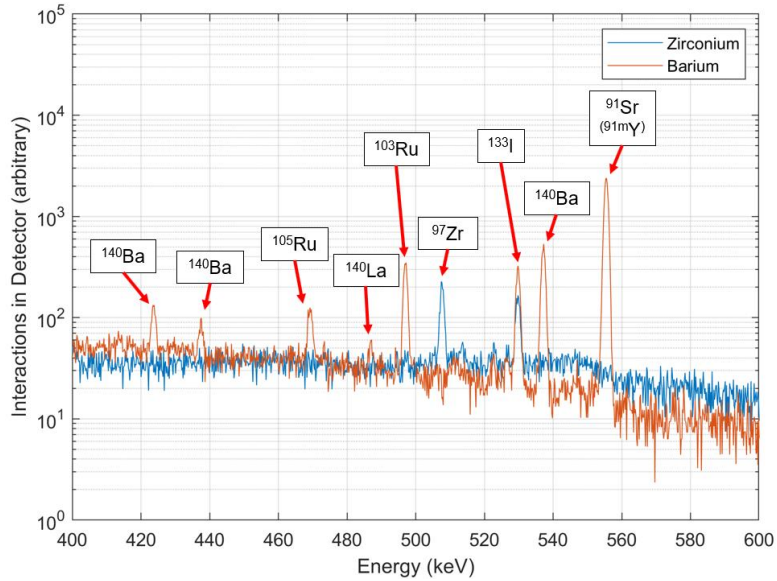
157 addition to Zr. The half-life for ^{97m}Nb is very short (52.7 seconds), so it is unobservable
158 in the molybdenum solution due to its separation from its parent nuclide, ^{97}Zr .



159

160 Figure 8. Comparison of gamma-ray spectra for fission product and molybdenum
161 solutions

162 In Figure 9, the comparison of zirconium and barium solutions are shown with very little
163 overlap between the isotopic constituents. As with all solutions, some iodine is
164 observable in each gamma-ray spectra.

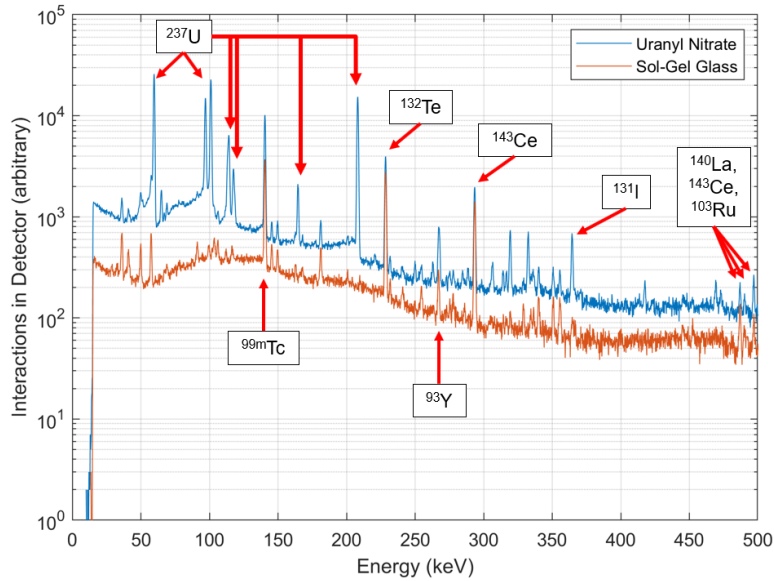


165

166 Figure 9. Comparison of gamma-ray spectra for zirconium and barium solutions

167

168 In Figure 10, the gamma-ray spectrum of the initial solution (uranium and all fission
169 products) is compared against the final gamma-ray measurement for sol-gel glass. The
170 ^{237}U , a result of (γ, n) reactions on ^{238}U during photon irradiation, is substantially reduced.
171 Many isotopes that are not specifically removed (Y, Ce, Ru) still exist. Importantly, the
172 sol-gel spectrum contains fission products of interest (e.g., ^{132}Te) and represents a
173 relatively small magnitude of x-rays (below 100 keV) as is representative of a sample
174 consisting of fission products without actinide content.

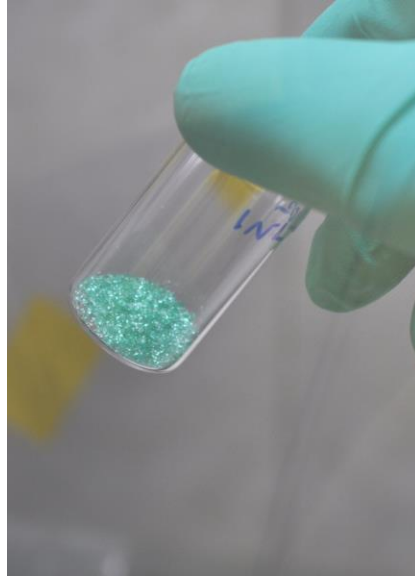


175

176 Figure 10. Comparison of gamma-ray spectra for uranyl nitrate solution and sol-gel glass

177

178 The final sol-gel particles in a vial are shown in Figure 11, with the coloration being
179 customized during the final steps of sol-gel production. Highlighted results from the sol-
180 gel glass are provided in Table 4, showing the agreement between desired values and the
181 measurement values within a coverage factor of 2.



182

Figure 11. Example of final product sol-gel glass

183

184

185 Table 4. Tabulated results for a single R-gamma value

Parameter	Desired Value	Measurement	Uncertainty ($k = 2$)
R -value $^{132}\text{Te}/^{99}\text{Mo}$	0.9	0.903	0.048
Effective Fissions	1.5×10^{12}	1.889×10^{12}	4.56×10^{11}

186

187 Conclusions

188 Gamma-ray spectrometry is used during production of surrogate nuclear debris to ensure
189 the desired result is achieved in terms of fission product ratios, total effective fissions,
190 and dose rate from the sol-gel sample. The detailed computational modeling of a specific
191 detector, including x-ray measurements, along with confirmatory measurements with
192 known laboratory standards allows for detector efficiency calculations for samples with
193 varying geometries and distances with simulations. The chemical separation of isotopes
194 can be imperfect, and a matrix-based approach to recombination of separated solutions
195 allows the final mixture to contain the desired isotope ratios without perfect isotopic
196 separation. The gamma-ray spectrometry of the final sol-gel particles is used to quantify,
197 with uncertainty, the R -values of interest and the effective fissions within the sample.

198 **Acknowledgements**

199 This research made use of Idaho National Laboratory computing resources which are
200 supported by the Office of Nuclear Energy of the U.S. Department of Energy and the
201 Nuclear Science User Facilities under Contract No. DE-AC07-05ID14517. INL is
202 operated for the U.S. Department of Energy by Battelle Energy Alliance under DOE
203 contract DE-AC07-05-ID14517. The authors would like to thank the U.S. Department of
204 Energy's National Nuclear Security Administration, Office of Defense Nuclear
205 Nonproliferation Research and Development, for financial support.

206

207 **References**

- 208 1. T. Goorley, et al., "Initial MCNP6 Release Overview," *Nuclear Technology*, **180**
209 (2012) p. 298-315.
- 210 2. D.A. Brown, et al., "ENDF/B-VIII.0: The 8th Major Release of the Nuclear Reaction
211 Data Library with CIELO-project Cross Sections, New Standards and Thermal
212 Scattering Data," *Nuclear Data Sheets*, **148** (2018) p. 1-142.
- 213 3. Jackman, K.R., "The Freiling Ratio and R-values," LA-CP-15-20429, Los Alamos
214 National Laboratory, 2015.
- 215 4. Jackman, K.R., Dry, D.E., Berning, D.E., Dale, D.E., Brooks, G.H., "Appendix B.
216 Early DFO Triage Time Measurements," LA-CP-15-20395, Los Alamos National
217 Laboratory, 2015.
- 218 5. Snow, M.S., Ward, J., Bucher, B., Cooper, J.T., Kinlaw, M., Cardenas, E., Horkley,
219 J., Town, H., Finck, M., Carney, K., "Rapid Separation of Photofissioned Uranium
220 Products via a Single-Pass Multiplexed Chromatographic Fission Product Separation
221 System, *Analytical Chemistry*," **(93)**8, p. 3770-3777, 2021.
- 222 6. Lefebvre, M., Keeler, R.K., Sobie, R., White, J., "Propagation of Errors for Matrix
223 Inversion," *Nuclear Instruments & Methods in Physics Research A* (**451**), p. 520-528,
224 2000.